

# Atomic layer deposition of solid-state electrolyte coated cathode materials with superior high-voltage cycling behavior for lithium ion battery application†

Cite this: *Energy Environ. Sci.*, 2014, 7, 768

Xifei Li,<sup>a</sup> Jian Liu,<sup>a</sup> Mohammad Norouzi Banis,<sup>a</sup> Andrew Lushington,<sup>a</sup> Ruying Li,<sup>a</sup> Mei Cai<sup>b</sup> and Xueliang Sun<sup>\*a</sup>

$\text{LiNi}_{1/3}\text{Co}_{1/3}\text{Mn}_{1/3}\text{O}_2$  (NMC) is a highly promising cathode material for use in lithium ion batteries; unfortunately, its poor cycling performance at high cutoff voltages hinders its commercialization. In this study, for the first time, we employ atomic layer deposition (ALD) to coat lithium tantalum oxide, a solid-state electrolyte, with varying thicknesses on NMC in an attempt to improve battery performance. Our results indicate that utilization of a solid-state electrolyte as a coating material for NMC significantly improves performance at high cutoff voltages but is strongly dependent on coating thicknesses. Our investigation revealed that a thicker coating proved to be beneficial in preventing cathode material dissolution into the electrolyte and aided in maintaining the microstructure of NMC. Consequently, a thicker ALD coating resulted in increased electrochemical impedance of the cathode. The results of this study indicate that an optimized coating thickness is needed in order to strike a balance between maintaining structural stability while minimizing electrochemical impedance. The coating thicknesses are functionally specific, and for the best improvement of a cathode, a particular coating thickness should be sought.

Received 9th August 2013  
Accepted 6th November 2013

DOI: 10.1039/c3ee42704h

www.rsc.org/ees

## 1. Introduction

$\text{LiNi}_{1/3}\text{Co}_{1/3}\text{Mn}_{1/3}\text{O}_2$  (NMC), a cathode material pioneered by Dr Ohzuku's and Dr Dahn's groups,<sup>1</sup> is comprised of alternating lithium and transition metal (111) layers, where the valence states of Ni, Mn, and Co are 2+, 4+, and 3+, respectively. During the electrochemical reaction between NMC and lithium, Ni participates as an electrochemically active species by alternating its oxidation state between 2+ and 4+, subsequently resulting in high energy capacity. Mn remains in the 4+ oxidation state throughout the electrochemical cycling process, and aids in maintaining outstanding cycle life and safety performance. Given the similar radius between  $\text{Ni}^{2+}$  (0.069 nm) and  $\text{Li}^+$  (0.076 nm), Co ion aids in preventing lithium and nickel ions mixing in the lattice while also increasing the overall electrical conductivity of NMC.<sup>2–5</sup> This mixed transitional metal ion cathode successfully integrates the advantages of  $\text{LiCoO}_2$ ,

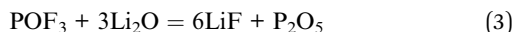
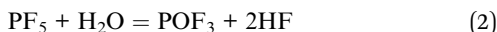
$\text{LiNiO}_2$  and  $\text{LiMnO}_2$ , and has garnered the attention of both fundamental scientists and applied researchers. Due to NMC's high capacity, low cost, enhanced cycling stability and high safety performance, it is regarded as a promising cathode material for application of LIBs in low-emission hybrid electric vehicles (HEVs) and plug-in hybrid electric vehicles (PHEVs).<sup>4,6</sup>

Recent publications have indicated that an increase in charge cutoff potential may also subsequently result in greater lithium extraction from NMC.<sup>1,7–9</sup> As a result, upper cutoff potentials have been progressively increased in an attempt to enhance the specific capacity obtained from NMC.<sup>9</sup> For instance, a linear increase in energy capacity has resulted from an increase in charge cut-off potentials above 4.2 V.<sup>8</sup> Given that, specific capacity  $\times$  average operating potential = energy density, an increase in the cutoff potential will result in increased LIB energy density. Unfortunately, charging the NMC cathode to higher cutoff potential results in significant deterioration in battery performance. Furthermore, when small amounts of moisture encounter salts contained within commercial LIB electrolytes, such as  $\text{LiPF}_6$ , the electrolyte begins to decompose while producing detrimental contaminants, which inevitably results in reduced electrochemical performance at high charge cut-off potentials. The following reaction scheme outlines byproducts formed by the decomposition of  $\text{LiPF}_6$ :<sup>10–13</sup>

<sup>a</sup>Nanomaterials and Energy Lab, Department of Mechanical and Materials Engineering, University of Western Ontario, London, Ontario, N6A 5B9, Canada. E-mail: xsun@eng.uwo.ca

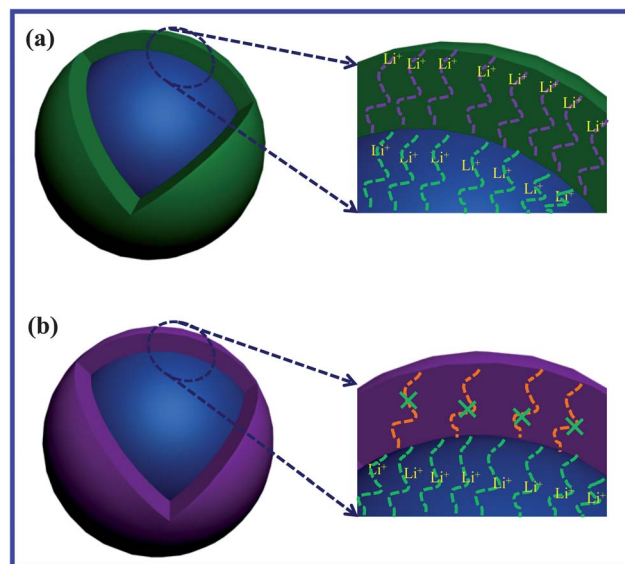
<sup>b</sup>General Motors R&D Center, Warren, MI 48090-9055, USA

† Electronic supplementary information (ESI) available: The atomic ratio between Ta and Ni, SEM images and elemental mappings, dark field image of HRTEM, the potentials of the redox peaks, cyclic performance at different potential ranges and its comparison at different temperatures. See DOI: 10.1039/c3ee42704h



Additionally, an increase in the upper cutoff potential would result in the acceleration of the above-mentioned reactions (1–3).<sup>8,14</sup> The interface between the cathode and liquid electrolyte plays a crucial role in the electrochemical reaction which subsequently results in energy storage.<sup>15</sup> The use of a high charge cutoff potential also results in increased surface reactivity between the electrolyte and the highly delithiated NMC material, leading to a dramatic increase in interfacial dissolution.<sup>9</sup> Therefore, the use of high charge cutoff potentials on NMC results in significant deterioration in cycling performance and rate capability,<sup>9,16–18</sup> hindering its potential application in HEV and PHEV batteries.

To address the issue of poor cycling performance and reduced rate capability, two important strategies are often utilized, the use of surface coatings and the incorporation of ion doping. Doped NMC has primarily been achieved by substituting metal ions or oxygen for either heteroatoms such as Mg, Ti, Al, Fe or anions such as F, in an attempt to provide enhanced structural stability while reducing cation mixing.<sup>19–23</sup> The other approach to enhancing NMC performance is the use of stable chemical surface coatings to prevent electrolyte/electrode interfacial reactions.<sup>24,25</sup> The utilization of this technique on NMC has proved to be a promising method for improving LIB cyclic performance.<sup>26–35</sup> The majority of efforts have been concentrated on the use of metal oxide surface coatings in an aim to reduce local dissolution of the NMC surface into the electrolyte.<sup>26</sup> Atomic layer deposition (ALD) is a surface-controlled and iterative monolayer-by-monolayer process, which relies on two sequential, self-terminating half-reactions.<sup>36,37</sup> The use of this technique enables the deposition of material precise angstrom-level thickness with excellent uniformity,<sup>10,38,39</sup> and demonstrates unique advantages in the application of surface coatings on LIB cathode and anode materials. Recently, a great deal of attention has been paid to metal oxide coatings performed by ALD including,  $\text{Al}_2\text{O}_3$ ,  $\text{TiO}_2$ , and  $\text{ZrO}_2$ . These coatings proved to highlight the significant advantages ALD can offer in enhancing the cyclic performance and rate capability for various cathode materials.<sup>10,28–35</sup> For example, Lee *et al.* demonstrated that an ALD coating of  $\text{Al}_2\text{O}_3$  on nano- $\text{LiCoO}_2$  electrode results in an elevated discharge capacity of  $133 \text{ mA h g}^{-1}$  at  $7.8 \text{ C}$ , representing a 250% improvement over non-coated nanoparticles.<sup>28</sup> Most importantly, Li *et al.* demonstrated that various metal oxide coatings,  $\text{TiO}_2$ ,  $\text{ZrO}_2$  and  $\text{Al}_2\text{O}_3$ , show different effects on the cycling performance and the rate capability of the  $\text{LiCoO}_2$  electrode: the  $\text{Al}_2\text{O}_3$  coating brings the best cycling stability while the  $\text{ZrO}_2$  coating contributes to the best rate capability.<sup>10</sup> However, due to the inherent properties of the metal oxides deposited by ALD, the coated materials often demonstrate reduced ionic conductivity, as well as hindered lithium ion transport into and out of the electrode particles, resulting in limited performance



Scheme 1 The difference between (a) solid state electrolyte coatings and (b) metal oxide coatings. The former provides higher lithium ion conductivity than the latter.

improvement.<sup>39</sup> By contrast, a solid-state electrolyte coating may overcome the limited lithium ion conductivity (see Scheme 1) seen in metal oxide coatings, and significantly increases the electrochemical performance of the coated material in LIBs.<sup>40–43</sup> So far, limited research efforts have been conducted on the effects that ALD derived solid-state electrolyte coatings have on NMC electrochemical performance.

Based on the significant advantages that metal oxide ALD coatings have to offer, we demonstrate the potential of using a solid-state electrolyte ALD coating,  $\text{LiTaO}_3$ , on the NMC cathode in an attempt to increase its capacity retention with cycling. To the best of our knowledge, we herein report for the first time an ALD derived solid-state electrolyte coating on an NMC cathode for performance improvement.

## 2. Experimental section

### 2.1 Preparation of the NMC electrode

The working electrodes were prepared by slurry casting on Al foils that served as current collectors. The slurry contained 80 wt% NMC cathode material, 10 wt% carbon black and 10 wt% poly(vinylidene) fluoride binder in the *N*-methylpyrrolidinone (NMP) solvent. The obtained electrodes were dried in vacuum at  $90 \text{ }^\circ\text{C}$  overnight.

### 2.2 $\text{LiTaO}_3$ coated NMC electrode

A solid-state electrolyte,  $\text{LiTaO}_3$ , was directly deposited on as-prepared NMC electrodes in an ALD reactor (Savannah 100, Cambridge Nanotechnology Inc., USA) at  $225 \text{ }^\circ\text{C}$  by sequential and alternate performing two subcycles as 1  $\text{Li}_2\text{O}$  subcycle and 6  $\text{Ta}_2\text{O}_5$  subcycles, where  $\text{Li}_2\text{O}$  resulted from alternate pulsing of lithium *tert*-butoxide ( $\text{LiO}^t\text{Bu}$ ,  $(\text{CH}_3)_3\text{COLi}$ ) (the source temperature  $T = 170 \text{ }^\circ\text{C}$ ) and  $\text{H}_2\text{O}$  ( $T = 23 \text{ }^\circ\text{C}$ ), and the  $\text{Ta}_2\text{O}_5$  subcycle

included alternate pulsing of tantalum ethoxide ( $\text{Ta}(\text{OEt})_5$ ,  $\text{Ta}(\text{OC}_2\text{H}_5)_5$ ) ( $T = 190^\circ\text{C}$ ) and  $\text{H}_2\text{O}$  ( $T = 23^\circ\text{C}$ ). During a typical ALD process, the pulse time of  $\text{LiO}^t\text{Bu}$  and  $\text{Ta}(\text{OEt})_5$  was 1 and 0.5 s, respectively, while  $\text{H}_2\text{O}$  was pulsed for 1 s. Precursor pulses were separated by a 10 s nitrogen gas purge. Nitrogen gas was also used as the carrier gas for all precursors with a flow rate of 20 sccm. The thicknesses of  $\text{LiTaO}_3$  coating layers were controlled by varying ALD cycles (0, 2, 5, 10 and 20), where the NMC cathode electrodes were coated by 0, 2, 5, 10 and 20-ALD-cycle  $\text{LiTaO}_3$  and are referred to as NMC-0, NMC-2, NMC-5, NMC-10, and NMC-20, respectively.

### 2.3 Characterization of the NMC electrode

X-ray powder diffraction (XRD) patterns were collected on a Bruker D8 Discover Diffractometer using  $\text{Co K}\alpha$  radiation ( $\lambda = 1.78897\text{ nm}$ ) at 40 kV and 40 mA. The morphologies and structures of various metal oxide thin film coating layers were observed by a field emission scanning electron microscope (FE-SEM, Hitachi S-4800), transmission electron microscope (TEM, Hitachi H-7000), and high-resolution transmission electron microscope (HRTEM, JEOL 2010 FEG). The Ta  $L_3$  edge X-ray absorption fine structure (XAFS) spectra measurements were performed on the 06ID superconducting wiggler sourced hard X-ray microanalysis (HXMA) beamline at the Canadian Light Source with a premirror-double crystal monochromator-post-mirror configuration using Si (111) crystals and Rh mirrors. The data were collected at the CLS 2.9 GeV ring operating at 175 mA injection current and the beamline wiggler running at 1.5 T. Measurements were made at room temperature in transmission mode for Ta foil with ion chambers filled with 100% of  $\text{N}_2$ , and in fluorescence mode for NMC-20 using a 32-element Ge detector.

### 2.4 Electrochemical testing of the NMC electrode

CR-2032-type coin cells were assembled in a glove box (Vacuum Atmosphere Company) under a dry argon atmosphere (moisture and oxygen level less than 1 ppm). The ALD coated electrodes and the lithium foils were used as the working electrodes and the counter electrodes, respectively. The electrolyte was composed of 1 M  $\text{LiPF}_6$  salt dissolved in ethylene carbonate (EC) : diethyl carbonate (DEC) : ethyl methyl carbonate (EMC) of 1 : 1 : 1 volume ratio. Cyclic voltammetry and electrochemical impedance spectroscopy tests were performed on a versatile multichannel potentiostat 3/Z (VMP3). Charge-discharge characteristics were galvanostatically tested between 3.0 and 4.5 V (vs.  $\text{Li}/\text{Li}^+$ ) at room temperature using an Arbin BT-2000 Battery Tester.

## 3. Results and discussion

It was demonstrated that ALD coatings deposited directly on cathode powders may result in slower  $\text{Li}^+$  diffusion and electron transport rates through the coating material.<sup>35</sup> Conversely, direct deposition of coating layers on cathode electrodes may result in maintaining electrical conductivity and enable rapid electron transport by avoiding deposition at contact points among active material particles, conductive agent, and the

current collector, which efficiently improves battery performance.<sup>35</sup> Given this information, we have decided to conduct all ALD depositions directly on the cathode electrode and reduce the inaccuracies that may arise from any uncoated material.

### 3.1 Morphology and structural characterization

As outlined in Fig. 1a(i), XRD diffraction peaks of NMC-0 exhibit sharp well defined Bragg lines corresponding to a rhombohedral structure, consistent with  $\alpha\text{-NaFeO}_2$  (space group:  $R\bar{3}m$ ). It is obvious that the existence of a secondary phase is negligible under the resolution utilized by the diffractometer. The XRD patterns of NMC-5, NMC-10, and NMC-20 are shown in Fig. 1a(ii-iv), respectively. The NMC electrodes coated with  $\text{LiTaO}_3$  by ALD show similar XRD patterns to that of NMC-0. This provides strong evidence that the ALD  $\text{LiTaO}_3$  coating process does not significantly alter the crystal structure of the NMC cathode or result in the formation of alternate NMC phases at the set deposited temperature. On the other hand, diffraction peaks corresponding to the  $\text{LiTaO}_3$  coating layer are absent in Fig. 1a(ii-iv) and may stem from two conditions: (1) the coating layers on the cathode electrodes are amorphously deposited; (2) the thickness of the coating layer exceeds the resolution of the XRD.

EDX of the coated NMC cathode was performed to analyze and confirm the presence of Ta, and is displayed in Fig. 1b. EDX spectra indicate that the Ta signal originates from the outside coating layer of the NMC electrode. Furthermore, EDX data indicate that Ta peak intensity increases with ALD cycle number

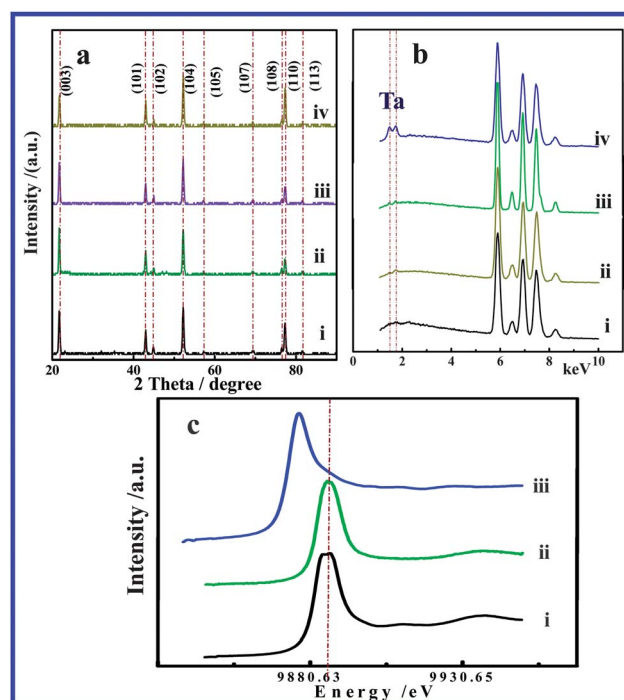


Fig. 1 (a) XRD patterns of (i) NMC-0, (ii) NMC-5, (iii) NMC-10, and (iv) NMC-20; (b) the EDX comparison of (i) NMC-2, (ii) NMC-5, (iii) NMC-10, and (iv) NMC-20; (c) Ta  $L_3$  edge structure in (i) NMC-20, (ii) the standard  $\text{LiTaO}_3$ , and (iii) the standard Ta metal.

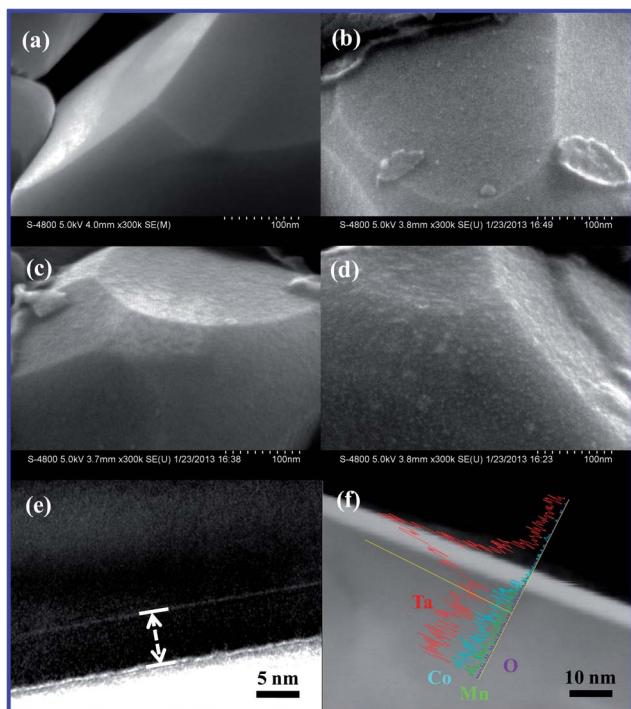


Fig. 2 Typical morphologies of (a) NMC-0, (b) NMC-2, (c) NMC-5, and (d) NMC-10; (e) HRTEM image and (f) linear scan of NMC-20.

and that the atomic ratio between Ta and Ni increases with the number of ALD cycles (see ESI Table S1†), providing further evidence towards increased coating layer thickness with ALD cycle number. The X-ray absorption near edge structure (XANES) provides geometric and electronic information within a distance of several angstroms around the targeted element

regardless of crystallinity.<sup>44</sup> XANES at the Ta  $L_{3}$ -edge was employed to investigate the local structure of the coating layer, as outlined in Fig. 1c. The spectra of standard  $\text{LiTaO}_3$  and pure Ta were also tested as a measure of comparison. Due to the electronic transition of unoccupied high-energy states near the Fermi level, one typical peak positioned at 9886 eV can be clearly observed in the spectrum of the standard  $\text{LiTaO}_3$  sample, which is in good agreement with previously reported values.<sup>45</sup> It is clearly evident that the Ta deposited by ALD has a peak with a similar chemical state to  $\text{LiTaO}_3$  compared to pure Ta metal. The slight peak shift and peak broadness for the Ta  $L_{3}$  edge of NMC-20 is a result of amorphous ALD deposition, further indicating the successful deposition of  $\text{LiTaO}_3$  by ALD.

The commercial NMC cathode material used in this study displayed monodispersed microspheres with a diameter of 5–20  $\mu\text{m}$  (see ESI Fig. S1a†). A close observation of the microspheres, shown in Fig. S1b,† revealed that they are in fact composed of smaller particles in a closely packed configuration with a diameter of around 400–900 nm. The lithium insertion process for layered cathode materials has previously been found to be a diffusion-dominated process.<sup>41,46,47</sup> As a result, smaller particles are capable of shortening lithium diffusion paths and thereby deliver enhanced battery performance. Fig. 2a shows a typical SEM image of NMC-0 at high magnification, demonstrating a clean and relatively smooth surface, being a typical characteristic of the pristine NMC particle. However, in Fig. 2b–d, the ALD process results in morphological changes to the NMC surface with the observation of a uniform and dense coating layer. Even for NMC-2, a coating layer can be clearly observed on the surface of the NMC electrode. Moreover, the thickness of coating layers increases with ALD cycle number, indicating a similar trend observed in previous research work conducted by our group. Furthermore, elemental mapping done by EDX

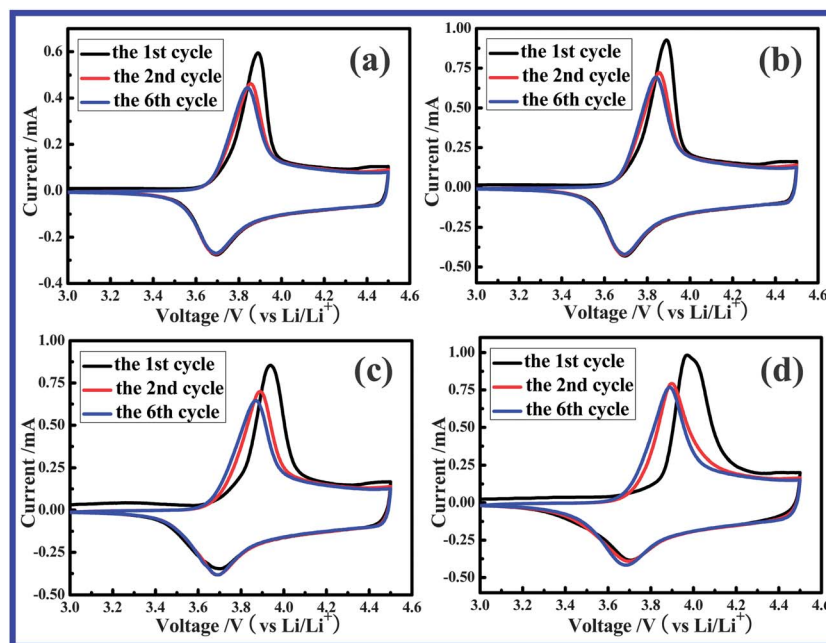


Fig. 3 Cyclic voltammograms of (a) NMC-0, (b) NMC-2, (c) NMC-5, and (d) NMC-10.

studies of  $\text{LiTaO}_3$  coated NMC electrodes reveals a uniform distribution of Ni, Co, and Mn in the cathode as well as Ta distribution in the coating layer on NMC (see ESI Fig. S2–5<sup>†</sup>). As shown in Fig. 2a, the pristine cathode exhibits relatively smooth surface characteristics while the coated cathode, in Fig. 2e and S6,<sup>†</sup> clearly shows a uniform coating layer with a thickness of 6.4 nm on the surface of NMC. An EDX line profile, scanned along the edge of the NMC coated material, shown in Fig. 2f, clearly indicates an increased presence of Ta around the edge of the particle and provides further confirmation of a  $\text{LiTaO}_3$  coating layer.

### 3.2. Li insertion/extraction behavior of NMC

Fig. 3a–d compares the CV profiles of NMC-0, NMC-2, NMC-5, and NMC-10 in the 1st, 2nd, and 6th scans cycled between 3.0 and 4.5 V (vs.  $\text{Li/Li}^+$ ), obtained by scanning at a sweep rate of  $0.1 \text{ mV s}^{-1}$ . The CV curves obtained for NMC cathodes with and without coating show typically observed redox peaks. The anodic (oxidation) peak is a result of the lithium extraction

process while the cathodic (reduction) peak denotes the lithium insertion process. The redox peak positions are summarized in Table S2.<sup>†</sup> In the first scan, the redox peaks of NMC-0 are centered at 3.890 and 3.696 V, giving a potential difference of 0.194 V. However, the potential difference between two peaks decreases to 0.163 in the second cycle and dips further to 0.148 V in the sixth cycle. For  $\text{LiTaO}_3$  coated NMC electrodes with varying ALD cycle number, a shift in both oxidation and reduction peaks can be observed, resulting in a larger difference between cathodic and anodic peaks (see ESI Table S2<sup>†</sup>). This leads to the conclusion that a high degree of electrochemical polarization occurs due to the low electrical conductivity of  $\text{LiTaO}_3$ . However, materials coated with fewer ALD cycles display a lower difference between peaks, indicating lower electrochemical polarization. This provides strong evidence that an optimized thickness of  $\text{LiTaO}_3$  coating is required to achieve increased cyclic performance for the NMC cathode.

As seen in the CV curves presented in Fig. 4a–c, it is clear that coating thickness has a pronounced effect on lithium diffusion into the cathode. Using an increasing scan rate of 0.1 between

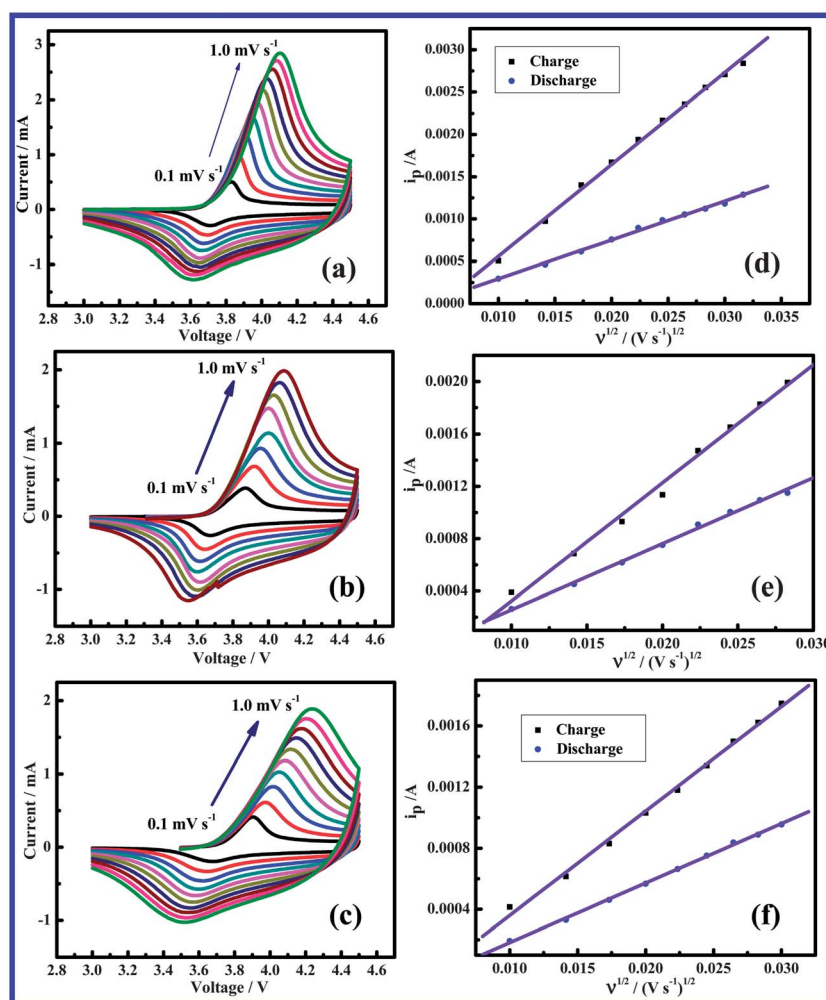


Fig. 4 The CVs of (a) NMC-0, (b) NMC-2, and (c) NMC-10 at various scan rates (0.1, 0.2, 0.3, 0.4, 0.5, 0.6, 0.7, 0.8, 0.9, and  $1.0 \text{ mV s}^{-1}$ ); dependence of peak currents as a function of the square root of scan rates in the charge and discharge region for three samples: (d) NMC-0, (e) NMC-2, and (f) NMC-10.

0.1 mV s<sup>-1</sup> and 1.0 mV s<sup>-1</sup>, a clear shift to higher and lower potential rates is observed with an increased scan between oxidation and reduction peaks respectively. The observed shift can be attributed to high electrochemical polarization occurring as a result of lithium diffusion rates within the cathode inadequately coping with increased CV scan rates. In Fig. 4a–c, the peak current ( $i_p$ ) is set as a function of the scan rate ( $\nu^{1/2}$ ) and can be expressed in the following equation:

$$I_p = 2.69 \times 10^5 \times n^{3/2} \times A \times D^{1/2} \times \nu^{1/2} \times \Delta C \quad (4)$$

where  $n$  is the number of electrons in the specific electrochemical reactions;  $A$  is the electrode area (cm<sup>2</sup>);  $D$  is the diffusion coefficient of lithium which needs to be calculated;  $\Delta C$  is the change in lithium concentration in the related reactions. Applying this equation to CV scan rates obtained for coated NMC materials, clearly a linear relationship exists between peak current and scan rate as shown in Fig. 4d–f, indicating diffusion-controlled behavior. Using the slope of the linear fits previously acquired, lithium diffusion coefficients in the cathodes can be calculated, and are presented in Table 1. Lithium diffusion values attained indicate that diffusion between non-coated and solid-state electrolyte coated NMC materials is similar, providing strong evidence that during the extraction/insertion process the ALD coating does not hinder lithium diffusion. This proves to be a significant advantage in using a solid-state electrolyte as a coating material.

### 3.3. Cycling performance and rate capability

As mentioned earlier, the energy density of LIB is dependent on the specific capacity and the working potential of electrode materials. The high cutoff potentials tested result in high specific capacity of NMC cathode materials.<sup>8,9,48</sup> As a result, increasing the cutoff potential is an important approach in enhancing LIB energy density.<sup>8,9</sup> To demonstrate the effect various cutoff potentials have on the cyclic performance of the NMC cathode, testing of assembled half-cells was conducted at various potential ranges and is shown in Fig. S7.† Clearly, an increase in specific capacity is achieved as the cutoff potential increases from 4.5 V to 4.6, 4.7 and 4.8 V. As shown in Table S3,† an increase in discharge capacity from 150 to 182 mA h g<sup>-1</sup> is observed with an increase in the upper cutoff potential from 4.5 to 4.8 V. Previous studies have indicated that the use of elevated current densities, such as 160 mA g<sup>-1</sup> on the NMC cathode results in a decrease in delivered capacity.<sup>49</sup> To highlight the advantages of using an ALD solid-state electrolyte, a current density of 160 mA g<sup>-1</sup> is applied to the NMC coated materials. However, a high cutoff potential results in accelerated electrode

degradation with cycling. At a current density of 160 mA g<sup>-1</sup>, an increased capacity fade is observed from 12% to 68% after 100 cycles for NMC-0 when the upper cutoff potential is increased from 4.5 to 4.8 V. In this study, ALD derived LiTaO<sub>3</sub> coatings were employed to study its effects on NMC cyclability at various potential ranges. Between the voltage range of 3.0 and 4.5 V, shown in Fig. 5a, all coated NMC materials indicated enhanced cyclability over non-coated NMC material. Interestingly, NMC-5 displayed better cyclability than NMC-10 and NMC-20. Furthermore, NMC-5 demonstrated an elevated discharge capacity of 145 mA h g<sup>-1</sup> with a high capacity retention of 93% in the 100th cycle. Based on the encouraging performance indicated by NMC-5 between the voltage range of 3.0 and 4.5 V, an explorative effort has been undertaken to investigate the effect the increased upper cutoff potentials of 4.6, 4.7 and 4.8 V have on the cyclability of ALD-coated NMC material. The results obtained from this study can be found in Fig. 5b–d. For the tested potential ranges of 3.0–4.6 V and 3.0–4.7 V, ALD coated material demonstrated a discharge capacity of 155 mA h g<sup>-1</sup> and 145 mA h g<sup>-1</sup> after 100 cycles, values similar to the ones obtained at the potential range of 3.0–4.5 V. This minimal difference in discharge capacity observed with the 5-ALD-cycle coated material demonstrates that this coating thickness may effectively protect the NMC electrodes from further degradation. Furthermore, the decreased cycling performance observed for the 10-ALD-cycle coated material provides strong evidence that high electrochemical polarization occurs with thicker LiTaO<sub>3</sub> layers. When the cut-off potential was further increased to 4.8 V, the reversible capacity of the NMC electrode rapidly declines, resulting in a low discharge capacity of only 59 mA h g<sup>-1</sup> at the 100th cycle, indicating serious cathode degradation occurring at the potential range of 3.0–4.8 V. During this situation, different from the other three potential ranges tested, NMC-10 shows the best effect on cyclability improvement with a higher discharge capacity of 122 mA h g<sup>-1</sup> and higher capacity retention of 73% after 100 cycles in comparison to NMC-0.

The commercialized NMC cathode studied in this paper displayed relatively good cyclability at room temperature, as shown in Fig. 5a. The cyclability of the cathodes at elevated temperature is limited as a result of increased surface phenomena of the cathode electrodes during cycles.<sup>50</sup> A comparison between the NMC cycle performance at room temperature and 55 °C is shown in Fig. S8,† and demonstrates that electrode degradation is much more pronounced at elevated temperatures. As previously reported,<sup>51</sup> a higher reversible capacity can be obtained at 55 °C due to increased lithium ion diffusion occurring at elevated temperatures. In this study, a solid-state electrolyte coating was employed to study its effect on cyclic performance at 55 °C. As shown in Fig. 5e, the ALD coated NMC electrodes demonstrate improved performance at 55 °C. Similar to the results obtained for cyclability at room temperature, NMC-5 indicated the highest discharge capacity of 167 mA h g<sup>-1</sup> while displaying a high capacity retention of 92% in the 100th cycle.

To demonstrate the advantages of using a solid-state electrolyte coating, rate capability of the coated NMC material was tested. As shown in Fig. 5f, the samples were charged and

**Table 1** Lithium diffusion coefficient (cm<sup>2</sup> s<sup>-1</sup>) of NMC-0, NMC-2, and NMC-10 in the charge and discharge regions

| State  | Charge                  | Discharge               |
|--------|-------------------------|-------------------------|
| NMC-0  | $3.502 \times 10^{-10}$ | $6.238 \times 10^{-11}$ |
| NMC-2  | $2.912 \times 10^{-10}$ | $7.543 \times 10^{-11}$ |
| NMC-10 | $1.387 \times 10^{-10}$ | $4.503 \times 10^{-11}$ |

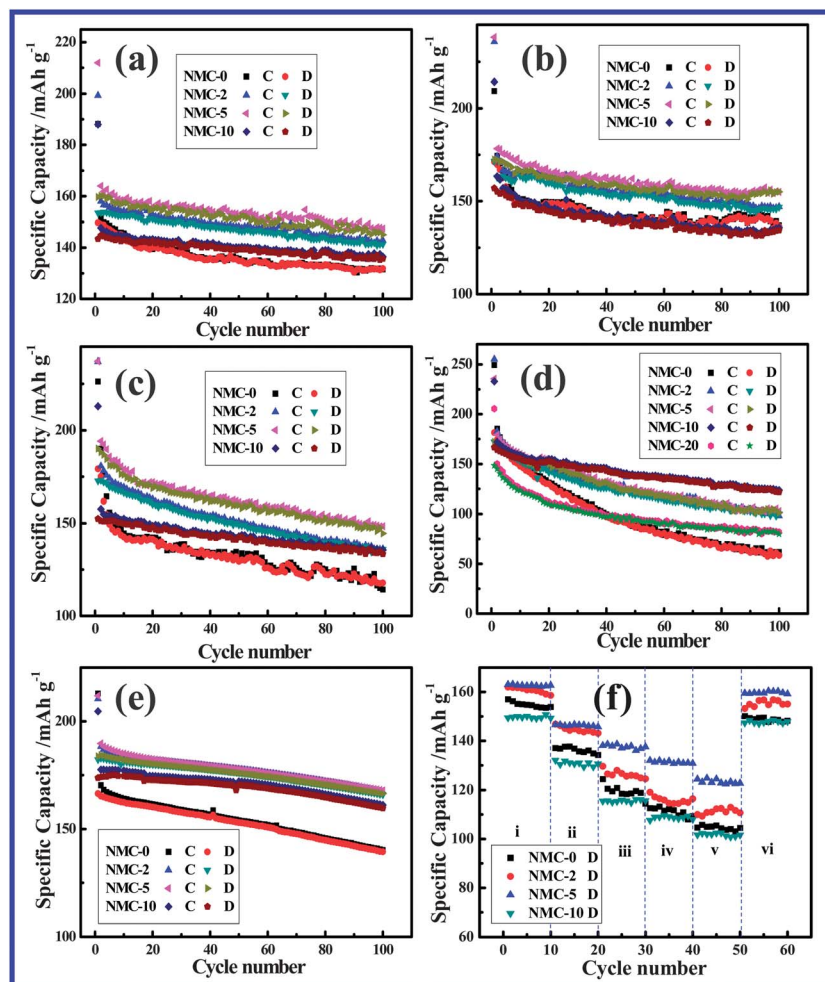


Fig. 5 The comparison of cyclic performance of NMC-0, NMC-2, NMC-5, NMC-10, and NMC-20 at a current density of 160 mA g<sup>-1</sup> at room temperature in the voltage range of (a) 3.0–4.5 V, (b) 3.0–4.6 V, (c) 3.0–4.7 V, and (d) 3.0–4.8 V; (e) cyclic performance of NMC-0, NMC-2, NMC-5, and NMC-10 at a current density of 160 mA g<sup>-1</sup> in the voltage range of 3.0–4.5 V at 55 °C; (f) rate capability of NMC-0, NMC-2, NMC-5, and NMC-10 at room temperature at various current densities: (i) 100, (ii) 300, (iii) 500, (iv) 600, (v) 700 and (vi) 100 mA g<sup>-1</sup>.

discharged using the current densities of 100, 300, 500, 600, and 700 mA g<sup>-1</sup>. For all cathode electrodes, the discharge capacities clearly decrease with increasing current density, a phenomenon typically observed in LIB electrodes.<sup>52,53</sup> Lithium ion diffusion inside the cathodes with very low behavior absolutely dominates the process of lithium insertion, which leads to a concentration gradient of the lithium ions in the cathodes during the discharge process. As a result, the cathode potential rapidly drops to the cutoff potential when the cathode surface completes the discharge process, while the central section of the cathodes could not complete the full discharge,<sup>54,55</sup> which results in the decrease of the cathode usage efficiency. The reduced efficiency of the cathodes will also occur when a higher current density is applied, inevitably resulting in lower discharge capacity. For all the current densities tested, NMC-5 shows the highest discharge from region i to vi. Even during the highest applied current density of 700 mA g<sup>-1</sup>, NMC-5 demonstrated a discharge capacity of 125 mA h g<sup>-1</sup>, 77% of the capacity seen at a current density of 100 mA g<sup>-1</sup>. Furthermore, NMC-5 displayed excellent reversibility by returning to a high

specific capacity following high-applied current density. The capacity comparison of all cathodes at various current densities is summarized and presented in Fig. S9† and further demonstrates that NMC-5 displays the best rate capability out of all samples tested.

#### 3.4. Analysis for performance improvement

As mentioned earlier, LiFP<sub>6</sub> electrolyte salt begins to decompose at elevated cutoff potentials *via* reaction 1–3, and results in the production of HF acid which in turn begins to corrode the NMC cathode.<sup>8,14</sup> To confirm the corrosion of the NMC cathode, dissolved transition metal ions (Mn, Co, and Ni) were examined after charge/discharge cycles between the voltage range 3.0 and 4.7 V followed by storing the electrode in LiFP<sub>6</sub> at 60 °C. ICP-AES was employed to quantitatively examine the amount of leaching of metal ions occurring from the cathode; the results are summarized in Table 2. By contrast, NMC-0 exhibited a much higher dissolution value for all three metal ions after storage. ALD coated materials displayed significantly decreased metal

**Table 2** The dissolution (ppm) of transition metal ions for NMC-0, NMC-2, NMC-5, and NMC-10 stored at 60 °C for 14 days estimated by ICP-AES analysis

| ALD cycle number | Mn dissolution | Co dissolution | Ni dissolution |
|------------------|----------------|----------------|----------------|
| 0c               | 547            | 491            | 425            |
| 2c               | 92             | 66             | 51             |
| 5c               | 58             | 36             | 31             |
| 10c              | 42             | 29             | 23             |

ion dissolution into the electrolyte. Furthermore, a thicker ALD coating resulted in less dissolution. Apart from metal ion dissolution, the cathode material may also undergo morphological changes with charge/discharge cycling at elevated cutoff potentials. The morphology of NMC-0 after 100 charge/discharge cycles using a 4.7 V cutoff was examined by SEM. The SEM image of the cycled NMC-0, as shown in Fig. 6a and b, clearly reveals a big difference from the morphology seen in Fig. 2a. Interestingly, previously unseen particles are observed on the surface of the NMC cathode, with a size of ~40 nm. Under HF acid attack, the structural degradation of the NMC cathode is triggered by the slow surface dissolution of the transition metal ions at the primary particle surface,<sup>56</sup> providing strong evidence for NMC-0 electrode degradation with charge/discharge cycles. Different from NMC-0, the LiTaO<sub>3</sub> coated NMC electrodes (NMC-2, NMC-5, and NMC-10) show a relatively small morphological change displayed in Fig. 6c–h in comparison to the pristine images. The results presented here give strong evidence that a solid-state electrolyte coating is effective in minimizing NMC leaching by the organic electrolyte and protecting the NMC electrode from structural degradation during the charge/discharge processes.

As previously mentioned, a LiTaO<sub>3</sub> coating may aid in protecting the cathode from harmful electrolyte degradation products upon cycling; however, existence of a coating layer may also adversely affect the electrochemical impedance of the NMC cathode. Electrochemical impedance spectroscopy (EIS) was employed to provide greater understanding as to the effects of using LiTaO<sub>3</sub> as a coating. EIS results obtained for NMC-0, NMC-5, and NMC-10 can be found in Fig. 7. All measurements were performed at 3.8 V during discharge at various cycles (say the 5th, 50th and 100th cycles). The obtained EIS consists of two depressed semicircles at high and medium frequency domains, followed by an inclined line in the low frequency region. The EIS of NMC-0 distinctly changes with the charge/discharge cycles. However, after ALD coating of LiTaO<sub>3</sub>, the electrodes show little EIS change on cycling. Importantly, the EIS of NMC-10 shows similar curves within three cycles. As expected, the EIS comparison in Fig. 7 indicates that the LiTaO<sub>3</sub> coating acts as a protective agent on the NMC cathode surface. A possible equivalent circuit is depicted in Fig. 7d to simulate the obtained curves. In the equivalent circuit,  $R_e$  represents ohmic electrolyte resistance. The first semicircle at high frequency is reflected by a resistor  $R_{s1}$  and a constant phase element  $CPE_{s1}$  relating to Li<sup>+</sup> migration through the surface film, while the second semicircle at lower frequency is due to the charge transfer reaction

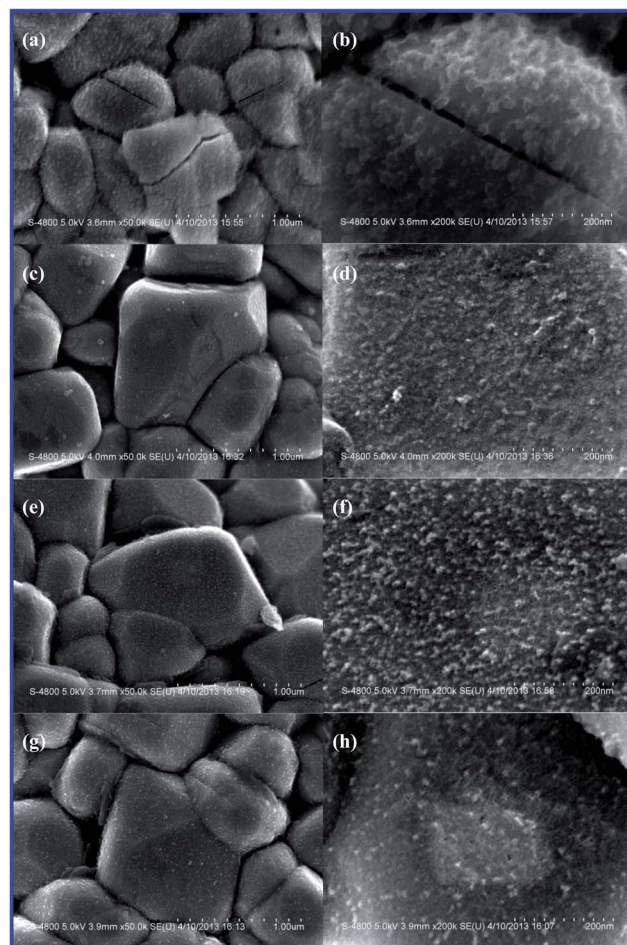


**Fig. 6** The morphology comparison of (a and b) NMC-0, (c and d) NMC-2, (e and f) NMC-5, and (g and h) NMC-10 after 100 charge/discharge cycles at a current density of 160 mA g<sup>-1</sup> at room temperature in the voltage range of 3.0–4.7 V.

represented by  $R_{ct}$  and the non-ideal double layer capacitance  $CPE_{dl}$ .  $W$  is the finite-length Warburg impedance that reflects the solid-state diffusion of Li<sup>+</sup> into the NMC cathode.<sup>57</sup> After simulation by the equivalently produced circuit, as shown in Table 3, it was found that  $R_{ct}$  of NMC-0 in the 100th cycle is 405 Ω, a value much higher than an  $R_{ct}$  of 54 Ω found in the 5th cycle. The value of  $R_{ct}$  of NMC-5 also increased with cycles, but its increasing trend is much lower than that of NMC-0. Furthermore, increasing the coating layer up to 10 ALD cycles shows a better protection effect with similar  $R_{ct}$  in the three cycles. However, it is noticeable that in the 5th cycle  $R_{ct}$  of NMC-5 and NMC-10 is higher than that of NMC-0. As one solid-state electrolyte, the electrical conductivity of LiTaO<sub>3</sub> is lower than that of the NMC cathode, thus LiTaO<sub>3</sub> coating increases the charge transfer resistance of the NMC cathode.

Based on the discussion above, a thicker solid-state electrolyte coating provides greater benefits for decreasing cathode dissolution into the electrolyte while maintaining the microstructure of NMC upon cycling. However, a thicker coating also results in an increase in the electrochemical impedance of the cathode. It is thus suggested that the coating thickness is

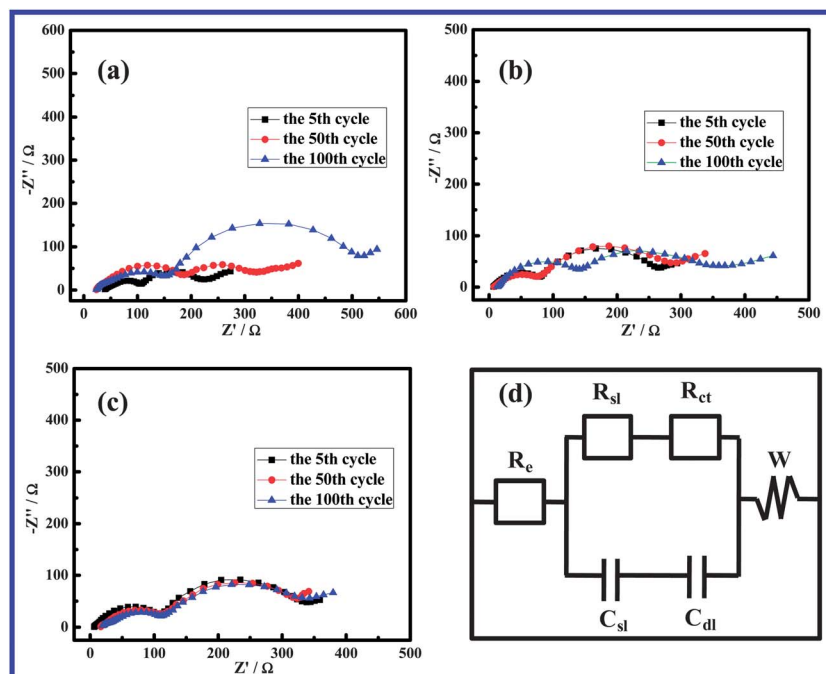


Fig. 7 Electrochemical impedance spectroscopy of (a) NMC-0, (b) NMC-5, and (c) NMC-10 in the 5th, 50th and 100th cycles; (d) a possible equivalent circuit is employed to simulate electrode reactions with lithium in Fig. 6a–c.

Table 3 Charge transfer resistance ( $R_{ct}$ ,  $\Omega$ ) of NMC-0, NMC-5, and NMC-10 at various cycles

| Samples | The 5th cycle | The 50th cycle | The 100th cycle |
|---------|---------------|----------------|-----------------|
| NMC-0   | 54            | 112            | 405             |
| NMC-5   | 147           | 184            | 200             |
| NMC-10  | 161           | 162            | 166             |

functionally specific, and for the best improvement of a cathode, a particular coating thickness should be sought. On the other hand, the  $\text{LiTaO}_3$  coating is different from other metal oxides. As it is well known, the inherent properties of metal oxides result in reduced ionic conductivity of the coated materials, which shows some limitation in the improvement of cathode performance. Most importantly, as shown in Scheme 1, this coating endows higher lithium ion conductivity than metal oxide coatings (see Table S4<sup>†</sup>),<sup>58</sup> thus the solid-state electrolyte coating provides a definite effect of the increase of the NMC cathode performance. For example, the cyclic performance of the NMC cathodes with 2-ALD-cycle derived coatings of the solid-state electrolyte ( $\text{LiTaO}_3$ ) and metal oxide ( $\text{TiO}_2$ ) is compared in Fig. S10,<sup>†</sup> obviously demonstrating that the solid-state electrolyte as an effective coating exhibits a significant effect in enhancing cathode performance in LIB application.

## 4. Conclusion

In summary, ALD allows for the deposition of uniform and dense lithium conductive  $\text{LiTaO}_3$  coating on the NMC

electrode surface with controllable layer thicknesses. We have studied the effects that solid-state electrolyte coating thickness have on the cyclic performance and rate capability of NMC cathode material in detail. Our study indicates that NMC-5 is effective towards improving cyclic performance of the cathode with an upper cutoff potential less than 4.8 V. Employing a cutoff potential of 3.0–4.8 V, NMC-10 indicates the best effect in decreasing NMC electrode degradation. However, with the use of a lower 3.0–4.5 V cutoff potential, NMC-5 exhibits extraordinary rate capability and cyclic performance at an elevated temperature of 55 °C. Therefore, the various behaviors seen in performance improvement not only demonstrated that ALD is a powerful technique to coat solid-state electrolytes on cathode materials, but also indicate that controllable coating thicknesses of solid-state electrolytes have a significant effect on cathode performance in LIBs.

## Acknowledgements

This research was supported by the Natural Science and Engineering Research Council of Canada (NSERC), General Motors of Canada, Canada Research Chair (CRC) Program, Canadian Foundation for Innovation (CFI), Ontario Research Fund (ORF), Early Researcher Award (ERA) and the University of Western Ontario. X. Li is grateful to Springpower International, Inc. and the MITACS Elevate Strategic Fellowship Program. We thank the friendly help from Dr. Ning Chen and Dr. Weifeng Chen at the Canadian Light Source (CLS) and Dr. Carmen Andrei at the Canadian Centre for Electron Microscopy of McMaster University.

## References

- W. Luo, X. Li and J. R. Dahn, *Chem. Mater.*, 2010, **22**, 5065–5073.
- H. Ren, Y. Wang, D. Li, L. Ren, Z. Peng and Y. Zhou, *J. Power Sources*, 2008, **178**, 439–444.
- H. Sclar, D. Kovacheva, E. Zhecheva, R. Stoyanova, R. Lavi, G. Kimmel, J. Grinblat, O. Girshevitz, F. Amalraj, O. Haik, E. Zinigrad, B. Markovsky and D. Aurbach, *J. Electrochem. Soc.*, 2009, **156**, A938–A948.
- L. Wang, J. Li, X. He, W. Pu, C. Wan and C. Jiang, *J. Solid State Electrochem.*, 2009, **13**, 1157–1164.
- H.-J. Noh, S. Youn, C. S. Yoon and Y.-K. Sun, *J. Power Sources*, 2013, **233**, 121–130.
- L. Wang, J. Li, X. He, W. Pu, C. Wan and C. Jiang, *J. Solid State Electrochem.*, 2009, **13**, 1157–1164.
- F. Zhou, X. Zhao, A. J. Smith and J. R. Dahn, *J. Electrochem. Soc.*, 2010, **157**, A399–A406.
- H. Zheng, Q. Sun, G. Liu, X. Song and V. S. Battaglia, *J. Power Sources*, 2012, **207**, 134–140.
- Y.-K. Sun, S.-W. Cho, S.-W. Lee, C. S. Yoon and K. Amine, *J. Electrochem. Soc.*, 2007, **154**, A168–A172.
- X. Li, J. Liu, X. Meng, Y. Tang, M. N. Banis, J. Yang, Y. Hu, R. Li, M. Cai and X. Sun, *J. Power Sources*, 2014, **247**, 57–69.
- T. Kawamura, S. Okada and J.-i. Yamaki, *J. Power Sources*, 2006, **156**, 547–554.
- W. Xu, S. S. S. Vegunta and J. C. Flake, *J. Power Sources*, 2011, **196**, 8583–8589.
- S. F. Lux, I. T. Lucas, E. Pollak, S. Passerini, M. Winter and R. Kostecki, *Electrochem. Commun.*, 2012, **14**, 47–50.
- B. R. Lee, H. J. Noh, S. T. Myung, K. Amine and Y. K. Sun, *J. Electrochem. Soc.*, 2011, **158**, A180.
- M. Hirayama, K. Sakamoto, T. Hiraide, D. Mori, A. Yamada, R. Kanno, N. Sonoyama, K. Tamura and J. Mizuki, *Electrochim. Acta*, 2007, **53**, 871–881.
- K. M. Shaju, G. V. Subba Rao and B. V. R. Chowdari, *Electrochim. Acta*, 2002, **48**, 145–151.
- H. Wang, Y. I. Jang, B. Huang, D. R. Sadoway and Y. M. Chiang, *J. Electrochem. Soc.*, 1999, **146**, 473–480.
- J. Li, M. Fan, X. He, R. Zhao, C. Jiange and C. Wan, *Ionics*, 2006, **12**, 215–218.
- W. Luo, F. Zhou, X. Zhao, Z. Lu, X. Li and J. R. Dahn, *Chem. Mater.*, 2010, **22**, 1164–1172.
- K. C. Kam, A. Mehta, J. T. Heron and M. M. Doeff, *J. Electrochem. Soc.*, 2012, **159**, A1383–A1392.
- F. Zhou, X. Zhao, Z. Lu, J. Jiang and J. R. Dahn, *Electrochem. Commun.*, 2008, **10**, 1168–1171.
- D. Liu, Z. Wang and L. Chen, *Electrochim. Acta*, 2006, **51**, 4199–4203.
- P. Yue, Z. Wang, H. Guo, X. Xiong and X. Li, *Electrochim. Acta*, 2013, **92**, 1–8.
- L. A. Riley, S. V. Atta, A. S. Cavanagh, Y. Yan, S. M. George, P. Liu, A. C. Dillon and S.-H. Lee, *J. Power Sources*, 2011, **196**, 3317–3324.
- Y. Wu, Z. Wen and J. Li, *Adv. Mater.*, 2011, **23**, 1126–1129.
- Z. Chen, Y. Qin, K. Amine and Y. K. Sun, *J. Mater. Chem.*, 2010, **20**, 7606–7612.
- G. Ting-Kuo Fey, C.-S. Chang and T. Kumar, *J. Solid State Electrochem.*, 2010, **14**, 17–26.
- I. D. Scott, Y. S. Jung, A. S. Cavanagh, Y. Yan, A. C. Dillon, S. M. George and S.-H. Lee, *Nano Lett.*, 2010, **11**, 414–418.
- H.-M. Cheng, F.-M. Wang, J. P. Chu, R. Santhanam, J. Rick and S.-C. Lo, *J. Phys. Chem. C*, 2012, **116**, 7629–7637.
- X. Luan, D. Guan and Y. Wang, *J. Nanosci. Nanotechnol.*, 2012, **12**, 7113–7120.
- J. Zhao and Y. Wang, *J. Phys. Chem. C*, 2012, **116**, 11867–11876.
- J.-T. Lee, F.-M. Wang, C.-S. Cheng, C.-C. Li and C.-H. Lin, *Electrochim. Acta*, 2010, **55**, 4002–4006.
- Y. S. Jung, P. Lu, A. S. Cavanagh, C. Ban, G.-H. Kim, S.-H. Lee, S. M. George, S. J. Harris and A. C. Dillon, *Adv. Energy Mater.*, 2013, **3**, 213–219.
- M. Bettge, Y. Li, B. Sankaran, N. D. Rago, T. Spila, R. T. Haasch, I. Petrov and D. P. Abraham, *J. Power Sources*, 2013, **233**, 346–357.
- Y. S. Jung, A. S. Cavanagh, L. A. Riley, S.-H. Kang, A. C. Dillon, M. D. Groner, S. M. George and S.-H. Lee, *Adv. Mater.*, 2010, **22**, 2172–2176.
- S. M. George, *Chem. Rev.*, 2009, **110**, 111–131.
- X. Meng, X.-Q. Yang and X. Sun, *Adv. Mater.*, 2012, **24**, 3589–3615.
- X. Li, X. Meng, J. Liu, D. Geng, Y. Zhang, M. N. Banis, Y. Li, J. Yang, R. Li, X. Sun, M. Cai and M. W. Verbrugge, *Adv. Funct. Mater.*, 2012, **22**, 1647–1654.
- D. J. Comstock and J. W. Elam, *J. Phys. Chem. C*, 2012, **117**, 1677–1683.
- J. Song, S. Jacke, D. Becker, R. Hausbrand and W. Jaegermann, *Electrochem. Solid-State Lett.*, 2011, **14**, A11–A13.
- N. J. Dudney, *J. Power Sources*, 2000, **89**, 176–179.
- K.-H. Choi, J.-H. Jeon, H.-K. Park and S.-M. Lee, *J. Power Sources*, 2010, **195**, 8317–8321.
- M. Surendra Kumar, J. Nanda, Y. Kim, R. Unocic, S. Pannala and N. Dudney, *J. Mater. Chem. A*, 2013.
- H. Asakura, T. Shishido, S. Yamazoe, K. Teramura and T. Tanaka, *J. Phys. Chem. C*, 2011, **115**, 23653–23663.
- S. H. Lee, I. Y. Kim, T. W. Kim and S. J. Hwang, *Bull. Korean Chem. Soc.*, 2008, **29**, 817–821.
- N. Meethong, Y.-H. Kao, W. C. Carter and Y.-M. Chiang, *Chem. Mater.*, 2009, **22**, 1088–1097.
- Y.-I. Jang, B. J. Neudecker and N. J. Dudney, *Electrochem. Solid-State Lett.*, 2001, **4**, A74–A77.
- J. Li, R. Klöpsch, M. C. Stan, S. Nowak, M. Kunze, M. Winter and S. Passerini, *J. Power Sources*, 2011, **196**, 4821–4825.
- A. M. A. Hashem, A. E. Abdel-Ghany, A. E. Eid, J. Trottier, K. Zaghbi, A. Mauger and C. M. Julien, *J. Power Sources*, 2011, **196**, 8632–8637.
- D. Aurbach, Y. Talyosef, B. Markovsky, E. Markevich, E. Zinigrad, L. Asraf, J. S. Gnanaraj and H.-J. Kim, *Electrochim. Acta*, 2004, **50**, 247–254.

- 51 P.-Y. Liao, J.-G. Duh and J.-F. Lee, *J. Power Sources*, 2009, **189**, 9–15.
- 52 X. F. Li, J. Liu, Y. Zhang, Y. L. Li, H. Liu, X. B. Meng, J. L. Yang, D. S. Geng, D. N. Wang, R. Y. Li and X. L. Sun, *J. Power Sources*, 2012, **197**, 238–245.
- 53 X. F. Li and Y. L. Xu, *Appl. Surf. Sci.*, 2007, **253**, 8592–8596.
- 54 K. Dokko, N. Nakata and K. Kanamura, *J. Power Sources*, 2009, **189**, 783–785.
- 55 H. Buqa, D. Goers, M. Holzapfel, M. E. Spahr and P. Novák, *J. Electrochem. Soc.*, 2005, **152**, A474–A481.
- 56 S.-H. Lee, C. S. Yoon, K. Amine and Y.-K. Sun, *J. Power Sources*, 2013, **234**, 201–207.
- 57 X. Li and Y. Xu, *Electrochem. Commun.*, 2007, **9**, 2023–2026.
- 58 J. Liu, M. N. Banis, X. Li, A. Lushington, M. Cai, R. Li, T.-K. Sham and X. Sun, *J. Phys. Chem. C*, 2013, **117**, 20260–20267.